JOURNAL OF MATERIALS SCIENCE, 30 (1995) 2843–2848

Optimization of hot workability of an Al–Mg–Si alloy using processing maps

J. SARKAR, Y. V. R. K. PRASAD, M. K. SURAPPA
Centre for Advanced Study, Department of Metallurgy, Indian Institute of Science, Bangalore 560012, India

The hot workability of an Al–Mg–Si alloy has been studied by conducting constant strain-rate compression tests. The temperature range and strain-rate regime selected for the present study were 300–550 °C and 0.001–1 s^{-1}, respectively. On the basis of true stress data, the strain-rate sensitivity values were calculated and used for establishing processing maps following the dynamic materials model. These maps delineate characteristic domains of different dissipative mechanisms. Two domains of dynamic recrystallization (DRX) have been identified which are associated with the peak efficiency of power dissipation (34%) and complete reconstitution of as-cast microstructure. As a result, optimum hot ductility is achieved in the DRX domains. The strain rates at which DRX domains occur are determined by the second-phase particles such as Mg_2Si precipitates and intermetallic compounds. The alloy also exhibits microstructural instability in the form of localized plastic deformation in the temperature range 300–350 °C and at strain rate 1 s^{-1}.

1. Introduction

The understanding of hot workability of wrought aluminium alloys is essential in order to obtain a desirable combination of microstructure and properties during working and shaping of these alloys using various metal-forming processes. In recent years, the hot-working characteristics of aluminium and its alloys have been studied extensively using torsion, tensile and compression techniques, and the influence of hot deformation parameters on the hot workability and the development of microstructures has been reported [1–9]. The effect of small intermetallic particles on the hot workability of Al–4.5 wt% Mg–0.8 wt% Mn has been discussed by Castro-Fernandez and Sellars [10]. However, there are few reports [11, 12] on the effect of Mg_2Si precipitates and intermetallic particles on the hot workability of Al–Mg–Si alloys. In the present study we report our observations on the hot workability of an Al–Mg–Si alloy, when it is deformed under compression. In order to characterize the hot workability, the recently developed dynamic materials model [13, 14] has been used to develop processing maps. The effects of temperature and strain rate on hot workability have been discussed, together with the manifestation of instability, using the instability criterion [15, 16].

The processing maps are developed on the basis of the dynamic materials model developed by Prasad *et al.* [13], which is reviewed recently by Alexander [14]. In this model, the work piece is considered as a dissipator of the system and its constitutive equation describes the manner in which the energy is dissipated at any instant which is non-recoverable by the system. At any instant, the total power dissipated is considered to be the summation of two complementary parts: G content representing the temperature rise and J co-content representating the dissipation through metallurgical processes such as dynamic recrystallization (DRX) and dynamic recovery (DRV). The factor that partitions power between G and J is the strain-rate sensitivity, m, of flow stress. The J co-content is given by the expression [13]

$$J = \sigma\dot{\varepsilon}m/(m + 1) \quad (1)$$

where σ is the flow stress and, $\dot{\varepsilon}$ is the strain rate. For an ideal linear dissipator, $m = 1$ and $J = J_{max} = \sigma\dot{\varepsilon}/2$. The efficiency of power dissipation, η, is expressed as a dimensionless parameter

$$\eta = J/J_{max} = 2m/(m + 1) \quad (2)$$

The variation of efficiency with temperature and strain rate constitutes a processing map. The various domains in the map may be correlated with specific microstructural processes and applied to microstructural control. The continuum criterion for the occurrence of microstructural instabilities [15, 16] is examined on the basis of the compression data. It has been shown that instabilities in microstructure will occur if

$$\xi(\dot{\varepsilon}) = \delta \ln[m/(m + 1)]/(\delta \ln\dot{\varepsilon}) + m < 0 \quad (3)$$

Microstructural instability is predicted to occur within the area bounded by the contour where $\xi(\dot{\varepsilon})$ is negative. At lower strain rates, the instability is less intense ($\xi(\dot{\varepsilon})$ is more positive). By superposing this instability map on the processing map, the area of instability can be delineated.

0022–2461

TABLE I Chemical composition (wt %) of the Al–Mg–Si alloy

Mg	Si	Cu	Cr	Mn	Fe	Other elements	Al.
1.7	0.6	0.3	0.2	0.23	0.2	0.22	Bal.

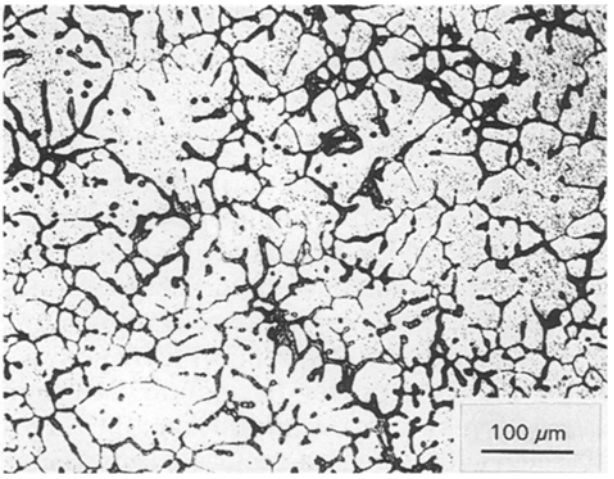

Figure 1 As-Cast microstructure of Al–Mg–Si alloy.

2. Experimental procedure

The chemical composition of the Al–Mg–Si alloy, in weight per cent, used in the present work, is shown in Table I. Fig. 1 shows the dendritic microstructure of a specimen in the as-cast condition. Specimens of diameter 10 mm and height 15 mm were made from as-cast cylindrical rods. A 0.8 mm diameter hole was drilled to a depth of 5 mm at half the height of each specimen for the insertion of a thermocouple. In order to understand the hot deformation behaviour, hot compression tests were carried out in a computer-controlled servohydraulic test system (DARTEC, UK). The lubrication was done with molybdenum disulphide and was made effective by engraving concentric grooves on both faces of the specimen. Specimens were tested at various constant strain rates, $\dot{\varepsilon}$, of 0.001, 0.01, 0.1 and 1.0 s^{-1} and the deformation temperatures were selected as 300, 350, 400, 450, 500 and 550 °C. In each case, the specimens were compressed to about half their height (50% strain, ε) and load–stroke data were converted into true stress–true plastic strain curves. The deformed specimens were immediately water quenched following the tests.

The procedure for obtaining processing maps was as follows: log (flow stress) versus log (strain rate) data at a constant temperature and strain are fitted using a cubic spline, and the strain-rate sensitivity, m, was calculated as a function of strain rate. This was repeated at different temperatures. The efficiency of power dissipation ($\eta = 2m/(m + 1)$) through microstructural changes, was then calculated from a set of values of m as a function of strain rate and temperature. Finally, iso-efficiency contours were plotted in the strain rate–temperature plane to develop two-dimensional power dissipation maps. The data were also used to evaluate the instability parameter $\xi(\dot{\varepsilon})$ (Equation 3) as a function of temperature and strain rate, and to obtain an instability map. The optical microscopy studies (grain size, volume per cent of precipitates etc.) were carried out in a section at the centre of the specimens parallel to the compression axis. Apart from Mg_2Si precipitates, intermetallic particles (size ≤ 1 μm, 1.6 vol %) were identified in the microstructure. Tensile specimens of gauge length 25 mm and diameter 4 mm were used for the constant strain-rate tests in the above temperature range. Fractured surfaces were analysed with the help of a scanning electron microscope (SEM).

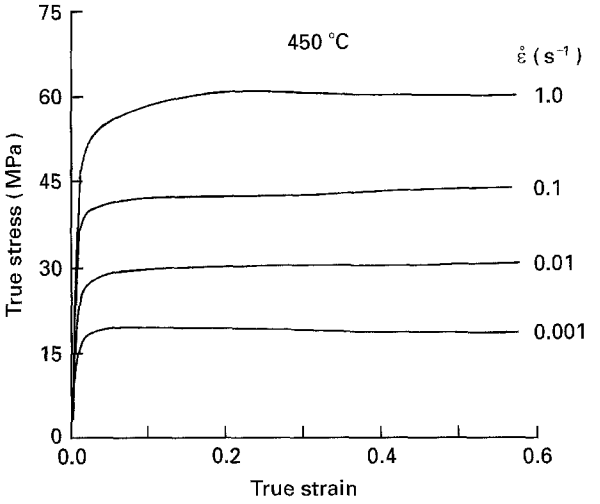

Figure 2 True stress–true strain curves for the Al–Mg–Si alloy at 450 °C.

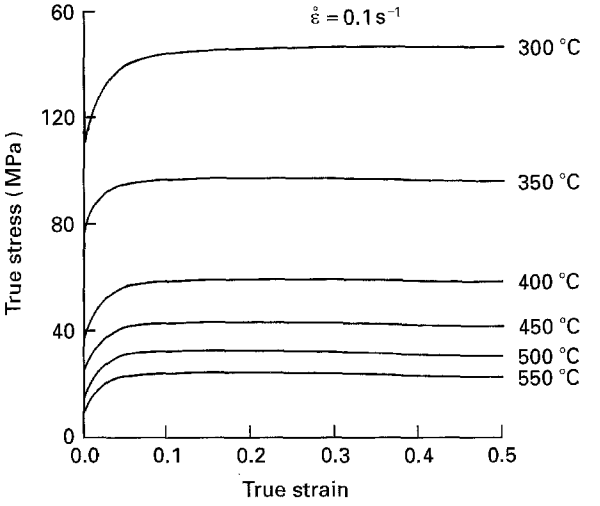

Figure 3 Isothermal true stress–true strain curves at a strain rate of 0.1 s^{-1}.

3. Results and discussion

Typical true stress–true strain curves recorded at 450 °C are shown in Fig. 2. These curves reveal near-steady-state flow behaviour within a strain rate regime of 0.001–1 s^{-1}. Fig. 3 exhibits the isothermal true stress–true strain curves at a constant strain rate of 0.1 s^{-1} for the alloy. The true stress values decrease progressively with increasing temperature. The values of true stress as a function of temperature and strain rate are listed in Table II. The values were corrected

TABLE II True stress values as a function of temperature and strain rate

Strain	$\dot{\varepsilon}(s^{-1})$	300 °C	350 °C	400 °C	450 °C	500 °C	550 °C
0.1	0.001	98.97	49.04	30.46	19.51	14.04	10.56
	0.01	113.44	72.40	43.06	30.95	22.07	14.36
	0.1	143.98	96.99	58.16	43.07	32.90	23.77
	1.0	160.23	109.28	76.35	60.94	45.87	37.93
0.2	0.001	97.31	48.94	31.87	19.87	14.49	10.27
	0.01	115.30	73.01	43.87	31.55	22.51	14.81
	0.1	147.54	97.03	60.61	44.49	33.69	24.58
	1.0	161.45	111.50	79.52	62.22	46.44	38.28
0.3	0.001	96.40	49.84	32.80	19.96	14.63	10.14
	0.01	117.08	73.50	43.55	32.17	22.78	15.38
	0.1	148.32	98.02	61.38	45.16	33.98	25.22
	1.0	162.14	112.61	80.26	61.97	46.46	38.00
0.4	0.001	95.98	51.00	32.80	20.49	14.69	10.46
	0.01	117.08	74.49	43.81	32.60	22.86	15.40
	0.1	149.47	100.56	62.32	45.60	34.03	25.65
	1.0	161.84	113.34	81.15	61.72	46.18	37.74
0.5	0.001	95.90	50.50	34.00	20.70	14.90	10.70
	0.01	119.87	74.00	44.00	32.70	23.50	15.60
	0.1	149.80	100.00	62.20	45.60	34.05	25.95
	1.0	161.35	112.50	81.20	61.95	46.45	38.05

for the adiabatic temperature rise using linear interpolation of $\log(\sigma)$ versus $(1/T)$ data at a constant strain rate.

It is obvious from Fig. 2 that the stress increases to a maximum up to a strain of 0.05 and remains nearly the same up to a strain of 0.5. This near-steady-state stress was found to be the main feature of true stress–true plastic strain curves at all the strain rates. Interestingly, neither single peak nor multi-peak stress oscillations were observed in the present study. This phenomenon can be explained based on the model proposed by Prasad and Ravichandran [17]. In the case of static recrystallization, the driving force is the fixed quantity of stored energy which must be released during annealing, whereas during hot compression energy is continuously fed into the material at a rate determined by the strain rate and temperature and this becomes dissipated through the softening process of DRX. Thus, energy input occurs through the generation of interfaces involving dislocations, and their recovery occurs by migration of interfaces. Consequently, the rate of generation of interfaces versus the rate of migration will decide the shape of the true stress–true plastic strain curves. If the rate of interface formation is equal to the rate of its migration, a steady-state flow curve will result. This is possibly the reason for near-steady-state flow in Al–Mg–Si alloy, but calculation of the rate of formation or rate of migration of interfaces is not possible at this stage due to the relatively high content of alloying elements.

3.1. Processing maps

The maps developed for the alloy using the dynamic materials model [13], at strains of 0.3 and 0.4 are shown in Fig. 4. The maps exhibit two distinct domains:

1. a domain centred at 550 °C and 0.02 s^{-1} (0.01–0.1 s^{-1}) with an efficiency of 34%;

2. another domain centred at about 450 °C and 0.001 s^{-1} with an efficiency of 34%.

These domains represent local order (concentric iso-efficiency contours) corresponding to specific dissipative mechanisms (microstructures) and can be interpreted in terms of specific atomistic processes. This is done with the help of Raj maps [18]. These two domains are identified as the domain of DRX for the present alloy. Fig. 5 shows the variation of efficiency of power dissipation with increasing temperature, at a constant strain rate of 0.02 s^{-1}. It is obvious from Fig. 5 that efficiency is maximum (34%) in the domain centred at 550 °C and 0.02 s^{-1}. Apart from efficiency, the hot ductility (reduction of area, RA) has been found to be maximum in the DRX domain (Fig. 5). The simultaneous occurrence of maximum efficiency of power dissipation and maximum ductility indicates the occurrence of DRX. Finally, DRX is confirmed by microstructural study which reveals strain-free grains (elongated in a direction perpendicular to the compression axis), essentially a feature of DRX. The microstructure of a specimen deformed at 550 °C and at a strain rate of 0.1 s^{-1} (Fig. 6a) shows a dynamically recrystallized grain structure with a mean grain size of 135 μm. Exactly similar observations have been made in the other domain centred at about 450 °C and 0.001 s^{-1} (Fig. 6b).

In the present alloy, second-phase particles (precipitates) have been observed in the microstructure (Fig. 6) which are identified as either Mg_2Si or stable intermetallic particles, such as $CuMg_4Al_6$, Fe_2SiAl_8, $(FeMn)_3SiAl_{15}$, etc. [19]. The mechanism of DRX is thought to be influenced by the presence of undeformable particles similar to that reported by Castro-Fernandez and Sellars [10] in Al–4.5 wt % Mg–0.8 wt % Mn alloy. The occurrence of DRX domain is expected to be a function of the interaction between particles and subgrains/dislocations. Very

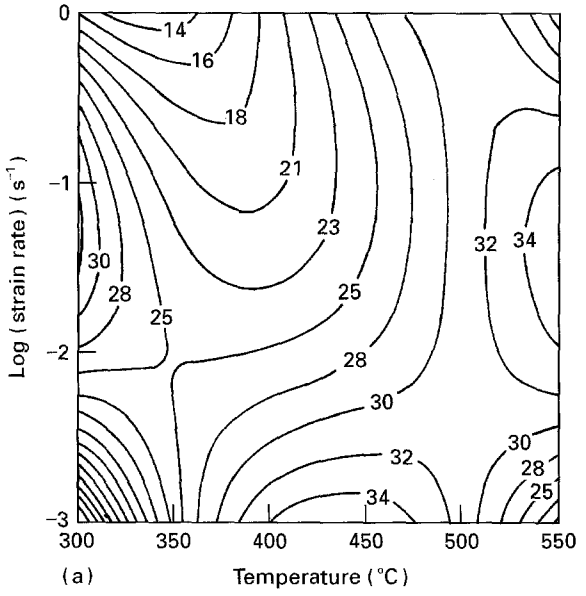

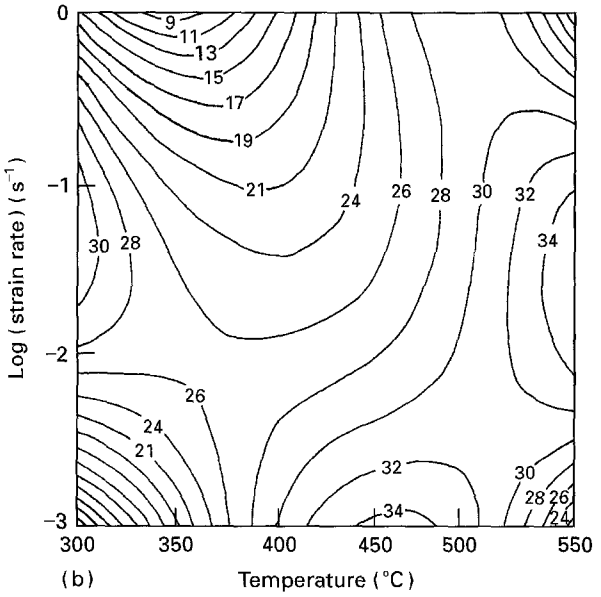

Figure 4 Processing maps for Al–Mg–Si alloy; variation of efficiency of power dissipation with temperature and strain rate, at a strain of (a) 0.3, and (b) 0.4.

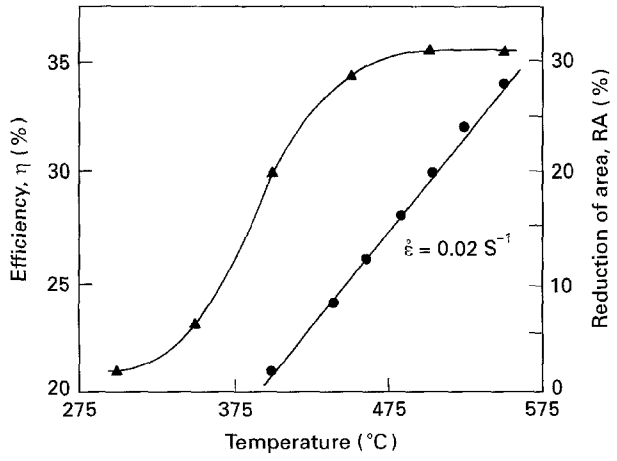

Figure 5 Variation of (●) efficiency of power dissipation, η, and (▲) ductility, RA, with temperature, at a strain rate of 0.02 s^{-1}.

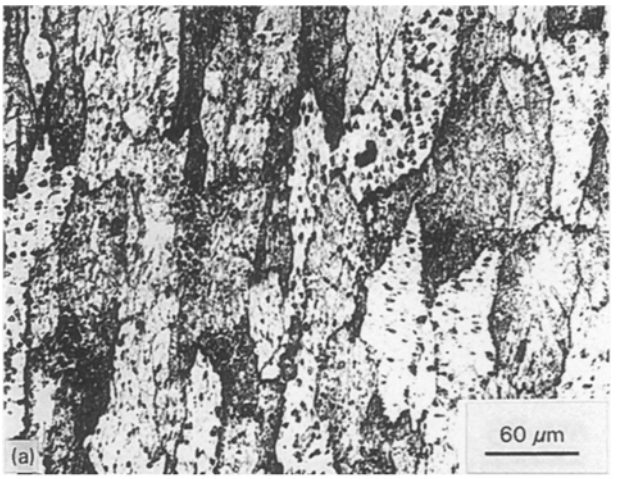

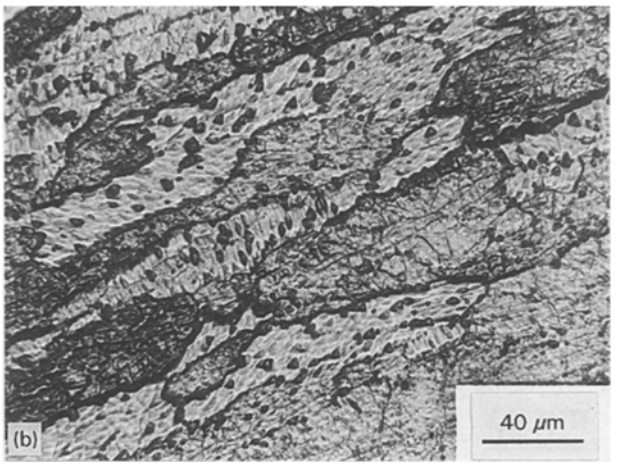

Figure 6 Microstructures of the deformed specimens (a) at 550 °C, 0.1 s^{-1}; (b) at 450 °C, 0.001 s^{-1}.

fine particles stabilize the subgrains by pinning the subgrain boundaries even at elevated temperature [2]; however, coarse particles enhance the tendency of recrystallization. Around these undeformable particles a region of high dislocation density (strain gradient) and large misorientation evolves into a small strain-free cell by a process of dislocation climb and rearrangement. Such a subgrain, once formed, can grow by sweeping up the dislocations in the volume it absorbs and leads to nucleation of strain-free DRX grains. In the present study, dissolution of Mg_2Si precipitates plays an important role in determining the strain requirement for DRX. At about 460 °C, both Mg_2Si and intermetallic particles exist and they effectively enhance the tendency of DRX even at very low strain rate (here 0.001 s^{-1}). However, Mg_2Si particles dissolve completely at 550 °C but intermetallic particles still remain at this temperature. Owing to the reduction in volume per cent of these particles, the strain-rate requirement is more for nucleation of DRX grains originated from increased boundary mobility. This is thought to be the reason for shifting DRX domain to a higher strain-rate regime (0.02 s^{-1}) with an increase in temperature.

Here, a comparison of Fig. 1 with Fig. 6 reveals that there is considerable reconstitution of microstructure in the deformed specimens due to DRX. It eliminates

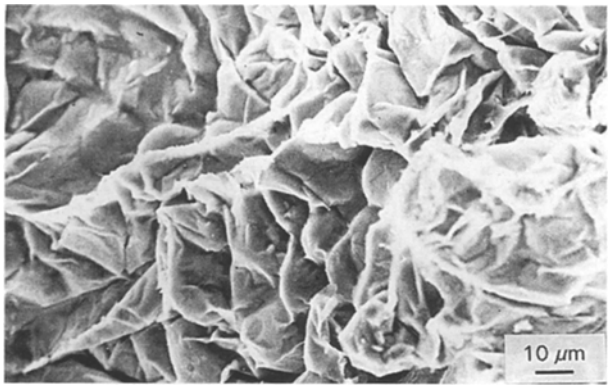

Figure 7 Scanning electron micrograph showing the fracture surface tested at 550 °C and 0.02 s^{-1}.

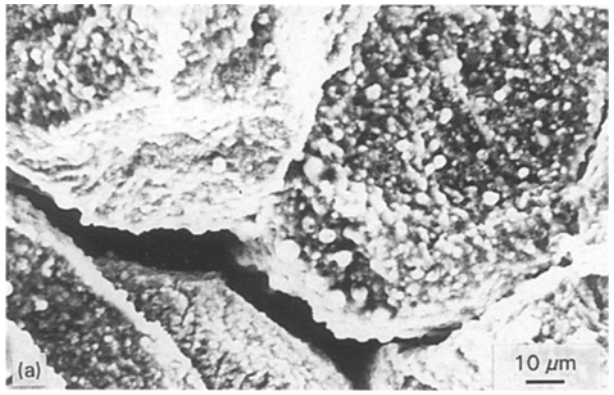

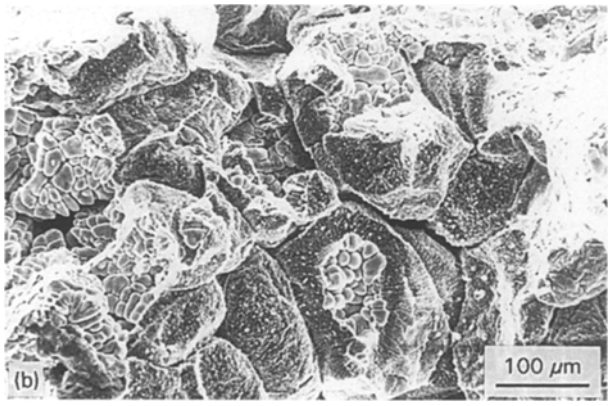

Figure 8 Scanning electron micrographs showing the fracture surface tested at 300 °C and 0.02 s^{-1}; (a) intergranular fracture; (b) interdendritic and intergranular fracture.

the cast structure and is replaced by a dynamically recrystallized microstructure which is aptly desirable for the structural application. Fig. 7 shows the fractograph (SEM) of the tensile specimen tested at 550 °C and 0.02 s^{-1}. The morphology indicates the ductile mode of fracture within the DRX domain. But, at 300 °C and 0.02 s^{-1}, both intergranular (Fig. 8a) and interdendritic (Fig. 8b) fracture have been identified and consequently the hot ductility is found to be low. Because, this combination of temperature and strain rate does not lie within the DRX domains, the microstructure has not been reconstituted completely and, as a result, dendrites are observed in the SEM fractograph. These observations illustrate the occurrence of reconstitution of microstructure (removal of cast

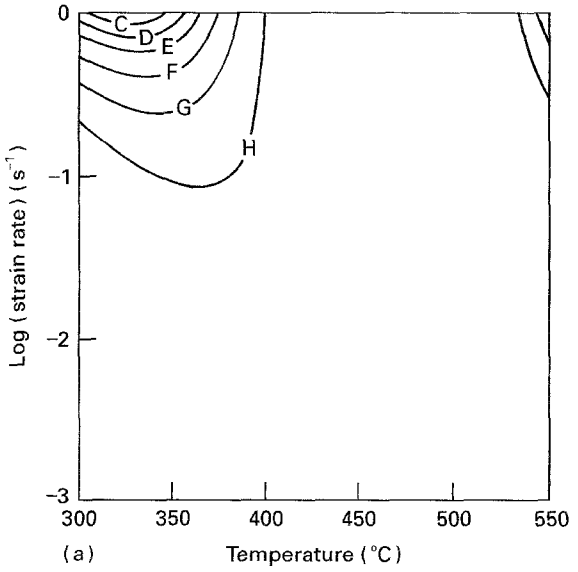

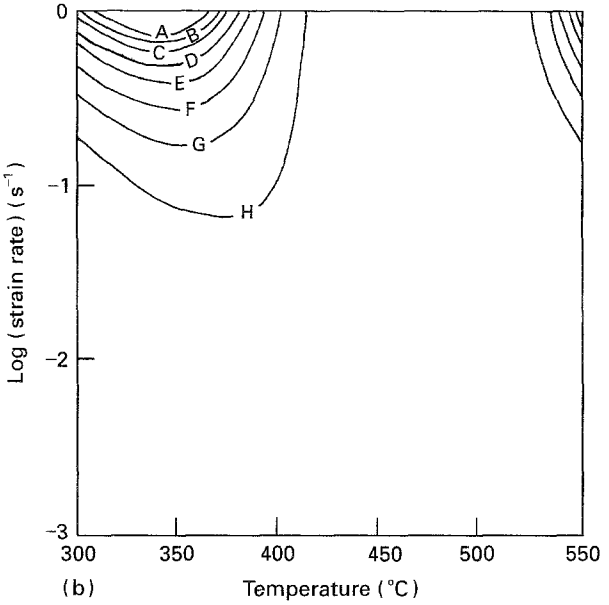

Figure 9 Instability maps for Al–Mg–Si alloy; variation of instability parameter, $\xi(\dot{\varepsilon})$, with temperature and strain rate, at a strain of (a) 0.3, and (b) 0.4. Levels A–H correspond to negative $\xi(\dot{\varepsilon})$ values of 0.88, 0.75, 0.63, 0.50, 0.38, 0.25, 0.13 and 0.00, respectively.

structure) within the DRX domains which results in improved hot ductility.

3.2. Instability maps

The variation of the instability parameter, $\xi(\dot{\varepsilon})$, with temperature and strain rate is shown in Fig. 9 for the Al–Mg–Si alloy at strains of 0.3 and 0.4. The domain of instability has been identified which is centred at 1 s^{-1} and 325 °C. Fig. 10 is an optical micrograph showing the instability at a strain rate of 1 s^{-1} and temperature of 300 °C. The instability is found to be due to the excessive plastic deformation of grains at high strain rate and low temperature.

Table III lists the temperature and strain-rate regimes of DRX and instability for Al–Mg–Si alloy.

4. Conclusions

An analysis of the hot deformation behaviour of the Al–Mg–Si alloy using the dynamic materials model in

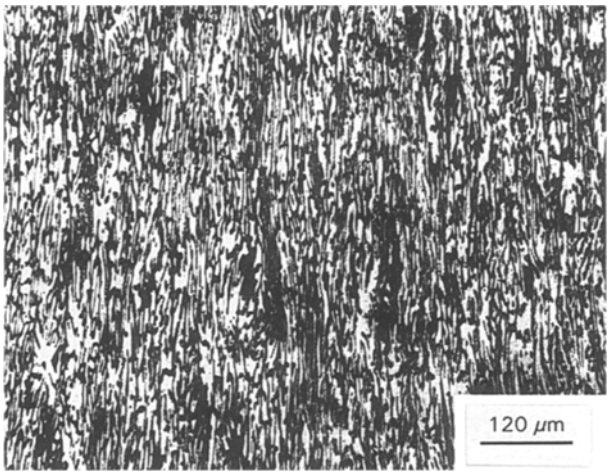

Figure 10 Microstructure of the Al–Mg–Si alloy specimen deformed at 350 °C and 1.0 s^{-1} (instability) reveals excessive plastic deformation of grains.

TABLE III Characteristic mechanisms as a function of temperature and strain rate

Processes	Temperature (°C)	$\dot{\varepsilon}$ (s^{-1})
Dynamic recrystallization	550	0.02
	450	0.001
Instability	300–350	1.00

the temperature range 300–550 °C and strain rate 0.001–1 s^{-1} leads to the following conclusions.

1. The isothermal true stress–true strain curves show either steady state or near-steady-state flow behaviour at all strain rates. The true stress value decreases progressively with an increase in temperature at a constant strain rate.

2. The Al–Mg–Si alloy undergoes DRX under suitable combinations of temperature and strain rate. Here, DRX occurs at two combinations of temperature and strain rate; one at 550 °C and 0.02 s^{-1} and the other at 460 °C and 0.001 s^{-1}.

3. The DRX domains are associated with the peak efficiency of power dissipation (34%) and maximum ductility (31% RA). Considerable reconstitution of the as-cast microstructure is observed during DRX and, consequently, the above parameters show the optimum hot workability.

4. The strain rates at which DRX domains occur are determined by the interaction between subgrain boundaries and Mg_2Si/intermetallic particles at respective temperatures.

5. At a temperature below 350 °C and a strain rate greater than 1 s^{-1}, microstructures exhibit microstructural instability which is manifested in the form of excessive plastic deformation.

This study suggests many additional experiments that could be performed to elucidate the hot deformation behaviour of this alloy. For example, differential scanning calorimetry (DSC) could be performed on the alloy tested in this study to identify the temperature at which phase changes (precipitation dissolution, etc.) occur. These DSC results could be supplemented with transmission electron microscope investigations to explain interaction between precipitates and dislocations.

Acknowledgements

The authors thank Mr S. Sasidhara, Metallurgy Department, for his assistance with the experiments. The Department of Science and Technology, India, is thanked for financial support during the course of the investigations.

References

1. H. J. McQUEEN, E. EVANGELISTA and N. D. RYAN, in "Proceedings of Recrystallization 90", edited by T. Chandra, (Metallurgical Society of AIME, Warrendale, PA, 1990) p. 89.
2. H. J. McQUEEN, in "Proceedings of Hot Deformation of Aluminium Alloys", edited by Langdon *et al.* (Minerals, Metals and Materials Society, 1991) p. 31, 105.
3. H. YAMAGATA, *Scripta Metall. Mater.* **27** (1992) 201.
4. H. J. McQUEEN and N. RYUM, *Scand. J. Met.* **14** (1985) 183.
5. M. RAGHAVAN and E. SHAPIRO, *Metall. Trans.* **11A** (1980) 117.
6. M. A. ZAIDI and T. SHEPPARD, *Met. Sci.* **16** (1982) 2229.
7. K. J. GARDENER and R. GRIMES, *ibid.* **3–4** (1979) 216.
8. T. SHEPPARD, N. C. PARSONS and M.A. ZAIDI, *ibid* **17** (1983) 481.
9. H. J. McQUEEN, E. EVANGELISTA and M. E. KASSNER, *Z. Metallkde* **82** (1991) 336.
10. F. R. CASTRO-FERNANDEZ and C. M. SELLARS, *Mater. Sci.* **4** (1988) 621.
11. A. ESPEDAL, H. GJESTLAND and N. RYUM, *Scand. J. Met.* **18** (1989) 131.
12. E. EVANGELISTA, A. FORCELLESE, F. GABRIELLI and P. MENGUCCI, in "Proceedings of Hot Deformation of Aluminium Alloys", edited by Langdon *et al.* (Minerals, Metals and Materials Society, 1991) p. 121.
13. Y. V. R. K. PRASAD, H. L. GEGEL, S. M. DORAIVELU, J. C. MALAS, J. T. MORGAN, K. A. LARK and D. A. BARKER, *Metall. Trans.* **15A** (1984) 1883.
14. J. M. ALEXANDER, "Modeling Hot Deformation of Steels: An Approach to Understanding and Behaviour" (Springer-Verlag, Berlin, 1989).
15. H. L. GEGEL, "Experimental Verification of Process Models" (ASM, Metals Park, OH, 1983).
16. A. K. S. KALYAN KUMAR, MS Thesis, Indian Institute of Science, Bangalore, India (1987).
17. Y. V. R. K. PRASAD and N. RAVICHANDRAN, *Bull. Mater. Sci.* **14** (1991) 1241.
18. R. RAJ, *Metall. Trans.* **12A** (1981) 1089.
19. L. F. MONDOLFO, "Aluminium Alloys: Structure and Properties" (Butterworths, London, 1976).

Received 21 April
and accepted 4 October 1994